Spectral Features and Charge Dynamics of Lead Halide Perovskites: Origins and Interpretations

Sum, Tze Chien; Mathews, Nripan; Xing, Guichuan; Lim, Swee Sien; Chong, Wee Kiang; Giovanni, David; Dewi, Herlina Arianita

2016

Sum, T. C., Mathews, N., Xing, G., Lim, S. S., Chong, W. K., Giovanni, D., et al. (2016). Spectral Features and Charge Dynamics of Lead Halide Perovskites: Origins and Interpretations. Accounts of Chemical Research, 49(2), 294-302.

https://hdl.handle.net/10356/81492

https://doi.org/10.1021/acs.accounts.5b00433

Spectral Features and Charge Dynamics of Lead Halide Perovskites: Origins and Interpretations

TZE CHIEN SUM,*[,†] NRIPAN MATHEWS,[‡,§] GUICHUAN XING[†], SWEE SIEN LIM,[†,//] WEE KIANG CHONG,[†,//] DAVID GIOVANNI[†,//] AND HERLINA ARIANITA DEWI[§]

[†]*School of Physical and Mathematical Sciences, Nanyang Technological University, 21 Nanyang Link, 637371, Singapore*

[‡]*School of Materials Science and Engineering Nanyang Technological University Nanyang Avenue, 639798, Singapore*

[§]*Energy Research Institute @NTU (ERI@N), Research Techno Plaza, X-Frontier Block, Level 5, 50 Nanyang Drive, Singapore 637553*

[//]*Energy Research Institute @NTU (ERI@N), Interdisciplinary Graduate School Nanyang Technological University, Singapore*

RECEIVED ON DATE GOES HERE.

CONSPECTUS

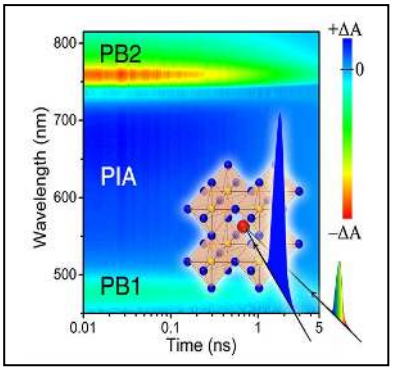

Lead halide perovskite solar cells are presently the forerunner amongst the 3rd generation solution-processed photovoltaic technologies. With efficiencies exceeding 20% and low production costs, they are prime candidates for commercialization. Critical insights into their light harvesting, charge transport and loss mechanisms have been gained through time-resolved optical probes such as femtosecond transient absorption spectroscopy (fs-TAS), transient photoluminescence spectroscopy, time-resolved terahertz spectroscopy and time-resolved microwave conductivity. Specifically, the discoveries of long balanced electron-hole diffusion lengths and gain properties in halide perovskites underpin their significant roles in uncovering structure-function relations and providing essential feedback for materials development and device optimization. In particular, fs-TAS is becoming increasingly popular in perovskite characterization studies, with commercial one-box pump-probe systems readily available as part of a researcher's toolkit. Although TAS is a powerful probe in the study of charge dynamics and recombination mechanisms, its instrumentation and data interpretation can be daunting even for experienced researchers. This issue is exacerbated by the sensitive nature of halide perovskites where the kinetics are especially susceptible to pump fluence, sample preparation/handling and even degradation effects that could lead to disparate conclusions. Nonetheless, with end-users having a clear understanding of TAS's capabilities, subtleties and limitations, cutting-edge work with deep insights can still be performed using commercial setups as has been the trend for ubiquitous spectroscopy instruments like absorption, fluorescence and transient-photoluminescence spectrometers.

Herein, we will first briefly examine the photophysical processes in lead halide perovskites, highlighting their novel properties. Next, we proceed to give a succinct overview of the fundamentals of pump-probe spectroscopy in relation to the spectral features of halide perovskites and their origins. In the process, we emphasize some key findings of seminal photophysical studies and draw attention to the interpretations that remain divergent and the open questions. This is followed by a general description into how we prepare and conduct the TAS characterization of $CH_3NH_3PbI_3$ thin films in our laboratory with specific discussions into the potential pitfalls and the influence of thin film processing on the kinetics. Lastly, we conclude with our views on the challenges and opportunities from the photophysical perspective for the field and our expectations for systems beyond lead halide perovskites.

1. Introduction

The phenomenal rise of organic-inorganic lead halide perovskite solar cells with an unprecedented surge in efficiencies from ~4% to >20% within a mere 6 years, heralded a new exciting chapter for 3rd generation solution-processed photovoltaic cells. Although this family of perovskites has been around for several decades, optoelectronic applications[1,2] scarcely commenced until the 1990's; while their photovoltaic potential[3] only became apparent in 2009. Several pioneering perovskite photovoltaic works[4-7] that followed in 2012-2013 incited the present perovskite renaissance. In unison with device-centric developments, fundamental studies using ultrafast optical spectroscopy (UOS) techniques have been pivotal in uncovering crucial insights into their light harvesting, charge generation, recombination and transport mechanisms. Discoveries of long, balanced ambipolar charge diffusion lengths[8,9], high carrier mobilities and slow recombination[10,11] and ultralow optical gain thresholds[12] in organic-inorganic lead halide perovskites bear testimony to UOS's significant role in revealing structure-function relations and providing essential feedback for materials development and device optimization.

UOS techniques include femtosecond transient absorption spectroscopy (fs-TAS), transient photoluminescence spectroscopy, time-resolved terahertz spectroscopy and time resolved microwave conductivity. In particular, commercial fs-TAS systems are now readily available (*e.g.*, HELIOS™ (Ultrafast Systems), Transient Absorption Spectrometer™ (Newport Corporation), FemtoFrame II™ (IB Photonics), *etc*.) – forming an essential part of the characterization toolkit for many materials laboratories. While such ready-made kits are a welcome relief from the tedious setting up and can certainly bring an emerging research group up to speed, there is a growing concern that new postgraduate students and early career researchers may simply treat them as "black boxes" without clearly understanding their intricacies. Although TAS is a powerful probe of carrier dynamics and relaxation mechanisms, interpreting their data can be challenging even for experienced users, with analysis possibly lasting for extended periods. Such issues are particularly worrisome for lead halide perovskites because of their novel optical properties (*i.e.*, large absorption coefficients, low bimolecular recombination rates and seemingly high Auger recombination rates) as well as their highly sensitive nature to the experimental conditions (*e.g.*, pump fluence), fabrication and preparation and external environmental factors (*e.g.* humidity). Aggravated by compelling external factors like fierce competition between research groups in a soaring field and the strong urge for publishing novel findings, hurried reporting with less than meticulous sample preparation, handling, instrumentation, data collection and interpretation could potentially set a field back. In this Account, we briefly examine the photophysical mechanisms and their dynamics in the archetypical $CH_3NH_3PbI_3$ perovskites. Focusing on fs-TAS, we highlight the potential issues of the technique and some factors that could influence the dynamics in $CH_3NH_3PbI_3$. This could possibly reconcile some of the differing views on the TAS data and interpretation in the literature.

2. Brief Overview of the Photophysical Processes

$CH_3NH_3PbI_3$ belongs to the broad perovskite family with the ABX_3 formula where the eight corner-sharing $CH_3NH_3^+$ (A cation) and the octahedral $[PbI_6]^{4-}$ forms the cubic unit cell. Despite the organic constituents, this material retains its inorganic semiconductor characteristics with the conduction band minima from the hybridizations of Pb 6p orbitals and the valence band maxima from Pb 6s and I 5p orbitals.[13] $CH_3NH_3PbI_3$ possesses a fairly large absorption coefficient (>10^5 cm^{-1} at 500 nm)[8] comparable to CdTe and GaAs and approximately one order higher than crystalline Si.[14] The puzzling range of the exciton binding energies reported (*i.e.*, <10 meV to ~50 meV)[15] have led to a concerted international effort to identify the primary photoexcited species (excitons or free carriers) in $CH_3NH_3PbI_3$.[16,17] Direct measurements of the exciton binding energies using high magnetic fields[18] eventually revealed binding energies <16 meV at low temperatures and a few meV at room temperatures (within the detection limits of the technique). It is now firmly established that upon photoexcitation, the excitons formed spontaneously dissociate into free electrons and holes,[19] thereby accounting for the impressive performance of perovskite solar cells.

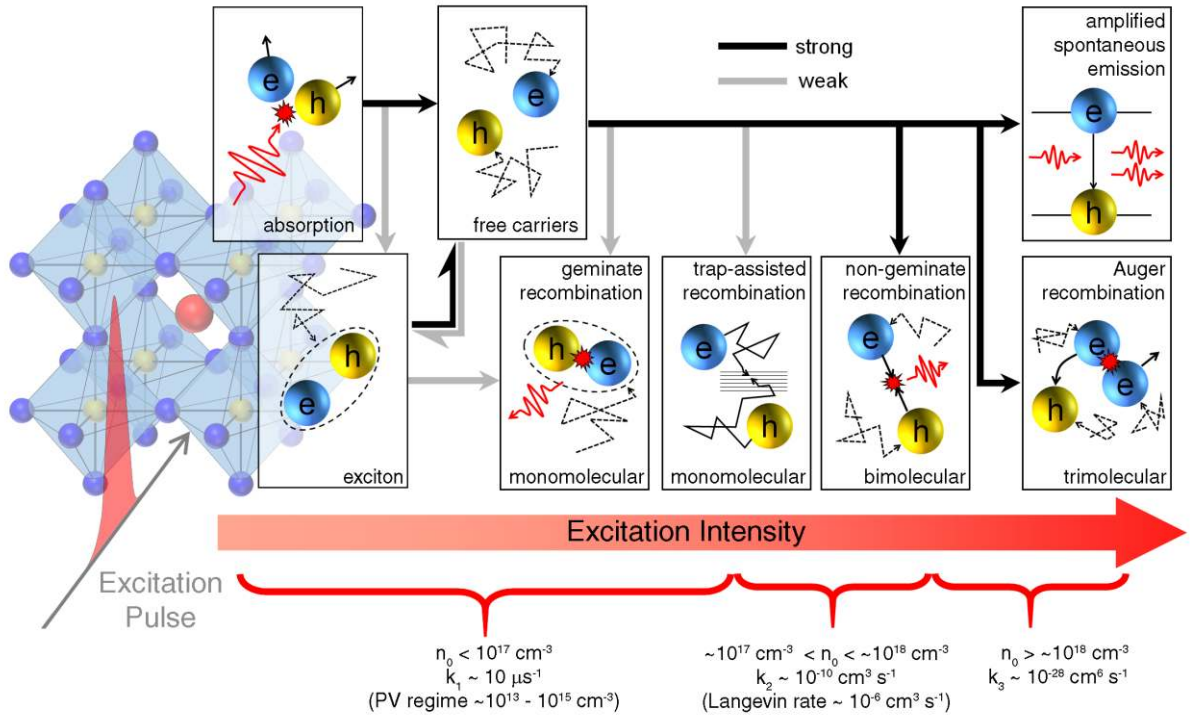

Figure 1 | Various photophysical processes and recombination rates in $CH_3NH_3PbI_3$ over a range of photoexcited carrier densities, n_0. Background schematic shows the typical $CH_3NH_3PbI_3$ perovskite structure.

Under low excitation fluence with carrier densities n_0 ~10^{13}-10^{15} cm^{-3} (*i.e.*, typical photovoltaic conditions), monomolecular processes like trap-assisted recombination or geminate recombination are found to be inefficient with low first order recombination coefficients k_1 ~10 μs^{-1}.[10] This agrees well with the relatively low trap densities (*i.e.*, n_{trap}~10^{17} cm^{-3}).[12] At higher n_0 ~10^{16}-10^{18} cm^{-3}, multi-particle effects like non-geminate

recombination (bimolecular) and Auger processes (tri-molecular) become more probable. Unlike geminate recombination that originates from the monomolecular annihilation of two coulombically bound charges, non-geminate recombination arises from the bimolecular recombination of two free charges. Surprisingly, their bimolecular recombination constants k_2 ~ 10^{-10} cm^3s^{-1} are approximately 4 orders lower[10,20] than the Langevin rates determined by assuming free electron-hole annihilation. However, their Auger rates[10] are found to be large (k_3 ~10^{-28} cm^6s^{-1}) – comparable to that of strongly confined CdSe colloidal quantum dots.[21] Recent works have found that $CH_3NH_3PbI_3$ undergoes strong band-filling effects[17,22] and bandgap renormalization[23] at higher pump fluence. Depending on the film quality, amplified spontaneous emission (ASE) could even be realized at n_0 ~10^{18} cm^{-3}, outcompeting the multi-particle processes. More exciting photophysics have recently been uncovered: correlated electron-hole plasma over the photovoltaic and stimulated emission fluences[17]; the slow hot carrier cooling[8] arising from a hot phonon bottleneck effect[23,24]; the microstructure size-dependence[25,26] of the electron-hole interaction and their carrier lifetimes; and the photoinduced refractive index changes[23]. This briefly summarizes some of the key findings of the seminal works and the latest developments on the photophysics of $CH_3NH_3PbI_3$ perovskites. For more detailed discussions, the interested reader is referred to more comprehensive reviews.[15,27-29]

2.1 Fundamentals of Femtosecond Transient Absorption Spectroscopy (fs-TAS)

Next, we provide a succinct description of fs-TAS, also known as pump-probe spectroscopy, specifically to highlight some of its essential components (Fig. 2(a)) that could unintentionally influence the data interpretation in $CH_3NH_3PbI_3$. There are many excellent references on the technique and data analysis where the interested reader can refer to for more details.[30,31]

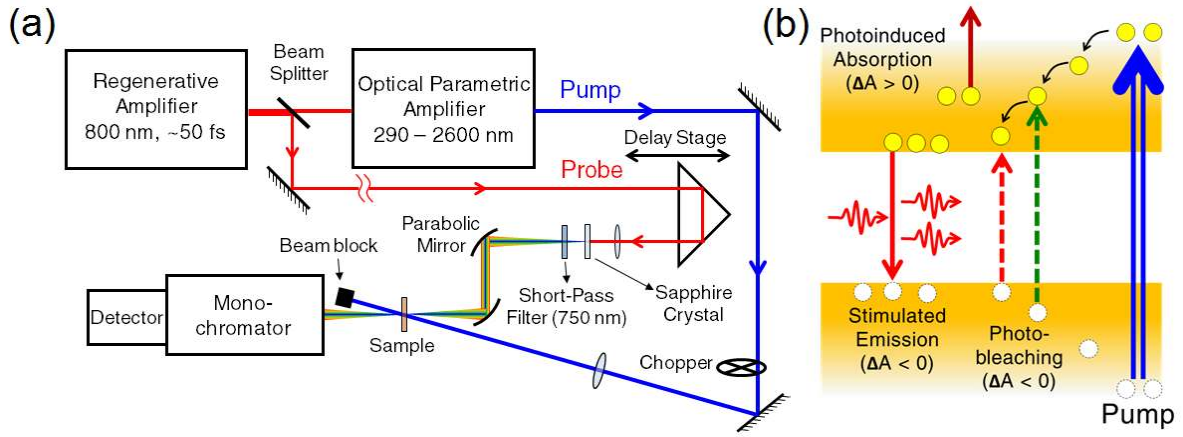

Figure 2 | (a) Typical layout of a non-degenerate fs-TAS setup with pump pulses from an OPA. The white light continuum (WLC) probe is generated by focusing a small amount of the fundamental 800 nm into a sapphire crystal. The 750 nm short pass filter (SPF) is absolutely essential in suppressing the residual 800 nm in the WLC for all $CH_3NH_3PbI_3$ studies. **(b)** An illustration of the photobleaching (PB), photoinduced absorption (PIA) and stimulated emission (SE) processes.

Briefly, TAS involves resonant excitation (or pumping) of electronic states, followed by a time-delayed probe with a weaker pulse (monochromatic or broadband white light continuum (WLC)) to interrogate the sample. The detector alternately measures the intensity of the probe pulse with pump on ($I(\lambda)_{\text{pump on}}$) or with pump off ($I(\lambda)_{\text{pump off}}$). The resultant absorbance difference spectrum ($\Delta A(\lambda) = -\log\left(\frac{I(\lambda)_{\text{pump on}}}{I(\lambda)_{\text{pump off}}}\right)$) consists of three types of signals:

- Photobleaching (PB) - $\Delta A < 0$; due to the reduction in optical density in the region of the ground state absorption from the depletion of ground state electronic population and filling of excited states;
- Stimulated emission (SE) - $\Delta A < 0$; due to the gain from transition from occupied excited electronic states to empty ground states;
- Photoinduced absorption (PIA) - $\Delta A > 0$; due to transition from newly occupied states to higher levels.

Data is collected by phase-sensitive techniques or by direct pulse storage methods using point or array detectors, and the time interval between the pump & probe pulses is set by controlling the optical paths with a delay stage. Rapid broad spectral probing with array detectors can be performed using a WLC probe. On the other hand, data collected using point detectors is more time consuming as it requires rotating the grating in the spectrometer over the wavelength range, but this scheme with lock-in detection affords better signal-to-noise (SNR) than array detectors. Array detectors are often employed in commercial systems and it is tempting to use a higher pump fluence to improve the SNR, but this could affect the kinetics and the subsequent interpretation. The wavelength dependence of the time-zero or the temporal overlap between the pump and the WLC probe beams also requires correcting for the chirp – a procedure that is readily integrated in commercial TAS systems. A 750 nm short pass filter (SPF) is typically used to suppress the residual 800 nm from the WLC generation. Typically, the WLC has an average power of only a few microwatts with the SPF in place. Such SPF may not be configured by default in commercial systems and one must ensure that it is present for all $CH_3NH_3PbI_3$ studies. Without the SPF, this residual 800 nm in the WLC is rather intense (with average power of ~200 μW) and could excite the $CH_3NH_3PbI_3$ sample through the bandedge or tail states (due to their broad bandwidth ± 10-15 nm femtosecond pulses) or through two-photon absorption. Some regenerative amplifiers are configured with a fundamental output of 775 nm (*e.g.*, Clark MXR-2010). Being more resonant with $CH_3NH_3PbI_3$ tail states, the absence of the SPF or any leakage of the residual 775 nm in the WLC probe in such configuration could lead to the inadvertent excitation of $CH_3NH_3PbI_3$.

2.2 Representative Transient Absorption Spectra of $CH_3NH_3PbI_3$

In our laboratory, fs-TAS experiments are either performed using our home-built TAS setup or a HELIOS™ TAS setup (Ultrafast Systems). In the former, the bulk of the fundamental 800 nm output from a Coherent Libra™ regenerative amplifier (50 fs, 1KHz, 4 mJ/pulse) is used for pumping the Coherent OPerA Solo™ optical parametric amplifiers (OPAs); while a fraction is used for WLC generation using a sapphire crystal. The pump beam from the OPA (*e.g.*, 600 nm) or from frequency doubling the fundamental 800 nm output (*e.g.*, 400 nm), are chopped at 83 Hz and the WLC probe signals are collected using a point detector with lock-in detection. For the HELIOS setup, the 800 nm pulses from a Coherent Legend™ regenerative amplifier (150 fs, 1KHz, 1 mJ/pulse), seeded by a Coherent Vitesse™ oscillator (100 fs, 80 MHz), is used to pump a TOPAS-C OPA to generate the pump beams. The pump beam is chopped at 500 Hz; while a small fraction of the 800 nm output from the Legend is fed to a sapphire crystal in the HELIOS for generating the WLC. The WLC probe signals are collected using array detectors. In both setups, a 750 nm SPF is placed in the probe path before the sample (Fig 2(a)) to filter out the residual 800 nm in the WLC. All TAS experiments were conducted with the sample in a dry nitrogen environment.

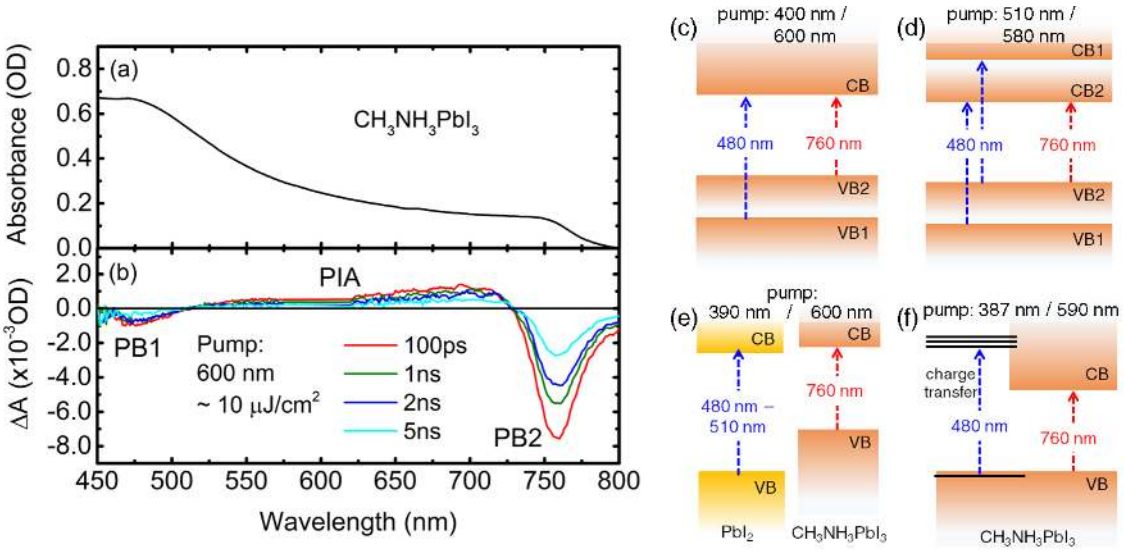

Figure 3 | Representative linear absorption spectrum **(a)** of $CH_3NH_3PbI_3$ showing the absorption edges at ~480 nm and ~760 nm and its TA spectrum **(b)** showing the PB1, PB2, and PIA signatures at various probe delays. Schematic of PB1 (480 nm) and PB2 (760 nm) contributions from: **(c)** dual valence band model;[8] (d) dual valence band and dual conduction band model;[32] and overlapping signals from **(e)** PbI_2;[33] and/or from **(f)** iodoplumbate complexes.[34]

Figure 3 shows a representative linear absorption and TA spectra of $CH_3NH_3PbI_3$. The latter was obtained with our HELIOS setup using a pump of 600 nm, fluence of ~10 μJ/cm^2. There are two distinct negative ΔA valleys located at approximately 480 nm and 760 nm (simply termed as PB1 and PB2, respectively) that originate from a combination of PB and SE signals. A broad positive ΔA (or PIA) band spans over the 550 nm to 650 nm wavelengths which is assigned to photoinduced refractive index changes.[23] The two PB signatures

coincide well with the two absorption edges present in the linear absorption spectrum that was previously assigned to excitonic transitions.[35] There is general consensus over the assignment of the bandedge signal PB2, but the origin of PB1 remains divergent. There are several interpretations: (i) dual valence band model[8], (ii) dual conduction band and dual valence band model[32], (iii) overlapping contributions from PbI_2 impurities[33] and (iv) from the charge transfer of iodoplumbate complexes in the fully formed $CH_3NH_3PbI_3$ (or dual excited states model)[34]. Recent first-principles band structure calculations[36,37] have partly supported (i) and (ii). For Fig 3(c), photoexcitation with energy less than PB1 (*i.e.*, with 600 nm pulses), the PB1 transition (blue dashed arrow) would correspond to the situation where only CB is populated – hence the dual valence bands. On the other hand, photoexcitation with energy less than PB1 (*i.e.*, with 510 nm or 580 nm pulses) in Fig 3(d), the PB1 transition (blue dashed arrows) would correspond to situations where only the higher energy valence band (VB2) or the lowest energy conduction band (CB2) are populated – hence the dual conduction bands and dual valence bands. Detailed discussions of the VB/CB assignments in (i) and (ii) can be found in the supplementary info of reference [8] and chapter 5 of reference [32], respectively. Here, we would like to urge the community to exercise caution as $CH_3NH_3PbI_3$ is highly sensitive to external environmental factors (*i.e.* humidity), sample handling and fabrication steps as well as experimental conditions during data acquisition. A combination of origins and/or external factors could possibly give rise to PB1 and influence the kinetics. Next, we will discuss some of the case studies conducted in our laboratory on the potential pitfalls in the TAS setup and the dependence on the sample preparation.

3. Case Studies

3.1. Sample Preparation

There are several reported fabrication methods for $CH_3NH_3PbI_3$ films. Broadly, the three main methods are: (a) single step deposition[4]; (b) two step deposition[6]; and (c) vapour deposition[7]. The most direct approach is (a), which involves spincoating a mixed solution of two precursors, CH_3NH_3I and PbI_2 in a polar solvent (*e.g.*, anhydrous dimethylformamide (DMF)) on substrates and followed by thermal annealing to form $CH_3NH_3PbI_3$. A variant involves dripping a second polar solvent (*e.g.*, chlorobenzene or toluene)[38] during the spincoating process to reduce the pinholes and obtain flat uniform films. For (b), a film of PbI_2 is first deposited on a mesoporous substrate and then dipped into a CH_3NH_3I solution for some time before completing the reaction with thermal annealing to form $CH_3NH_3PbI_3$. Lastly, (c) involves a dual source evaporation of two precursors where fine control of the process is needed to achieve the desired stoichiometric ratio. Here, we had adopted (a) where 78.3 mg/ml lead(II) iodide (Acros Organics PbI_2) and 27.0 mg/ml methylammonium iodide (DyeSol CH_3NH_3I) were dissolved in N,N-Dimethylformamide (Sigma Aldrich DMF) in a N_2-filled glovebox to obtain a clear yellow 10 wt.% $CH_3NH_3PbI_3$ solution. Neat films were obtained by spin-coating 20μL of the heated solution (70 ^oC) onto cleaned 1 mm-thick quartz substrates at 2000 RPM for 60 seconds and then annealed at 100 ^oC for 30 minutes. No solvent wash/dripping was performed. The quartz substrates were earlier cleaned with air-plasma for 10 minutes, then rinsed with de-ionised water and dried. The samples were

mounted in a sample holder inside a nitrogen glovebox and sealed for optical spectroscopy. Note the film preparation procedure here is different from our earlier work on the electron-hole diffusion lengths where the samples were annealed for 20s and then vacuum-stored for >3 days to rid of the residual solvent. Such differences in the film preparation have a strong influence on the crystal sizes and sample morphology. This resulted in some new observations in the 600 nm pumped TAS spectra – see discussion below.

3.2 Effects of Pump fluence and Inadvertent Excitation from the Residual 800 nm Fundamental in the WLC

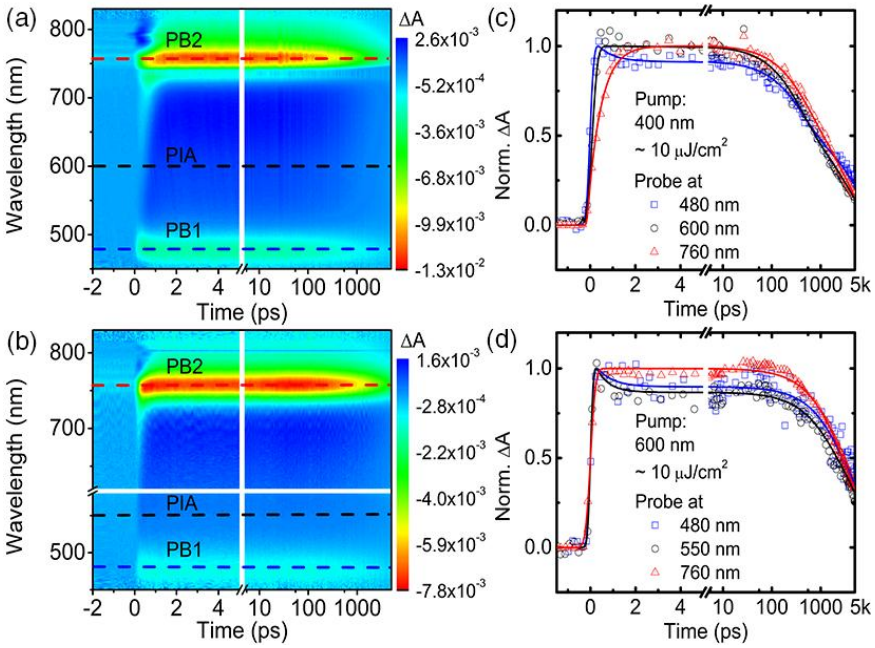

Figure 4| Pseudo-color TA plots at different probe wavelengths and probe delay times photoexcited with **(a)** 400 nm and **(b)** 600 nm femtosecond laser pulses with ~10 μJ/cm^2 fluence at 1 KHz repetition rate. The thick white lines in **(a)** and **(b)** are breaks in the temporal or spectra axis. These chirp-corrected data were collected using our HELIOS^{TM} (Ultrafast Systems) setup with SPF in the probe path. **(c)** and **(d)** shows a comparison of the kinetics at around 480 ± 5 nm, 550 ± 5 nm, 600 ± 5 nm and 760 ± 5 nm. The 480 nm and 760 nm kinetics are plotted as negative ΔA to allow comparison with the positive ΔA values at 550 nm or 600 nm.

Figure 4 shows the pseudo-color TA plots of the sample as a function of probe wavelengths and probe delay time after photoexcitation with 400 nm and 600 nm pump pulses at ~10 μJ/cm^2 pump fluence. The time evolution of the three main features of PB1 (480 nm), PB2 (760 nm) and PIA (550 nm or 600 nm) up to 5 ns are shown in Fig. 4(c) and 4(d). Note that the 480 nm and 760 nm kinetics are plotted as negative ΔA values to allow comparison with the positive 550 nm and 600 nm ΔA transients. In the first 1-2 ps (Fig. 4(c)) after 400 nm pump, the concomitant rise in the 760 nm trace (red line) and the decay in the 480 nm trace (blue line) was previously assigned to hot carrier cooling in the dual valence band model[8] where recent studies have pointed its origins to a hot-phonon bottleneck.[23,24] At the short timescales (<5 ps), the hot carrier cooling process is more apparent with the 400 nm

pump than with the 600 nm pump. Over the longer relaxation timescale, there are typically two lifetimes – a shorter pump-fluence dependent lifetime at several hundred ps originating from bimolecular recombination and a longer one at a few nanoseconds originating from trap-assisted monomolecular recombination. The former lifetime becomes apparent with pump fluence >7 μJ/cm^2 and it decreases with increasing photogenerated carrier densities. Nonetheless, at the same photogenerated carrier densities, one should obtain very similar relaxation dynamics in these perovskite thin films regardless of photoexcitation with 400 nm or 600 nm wavelengths.

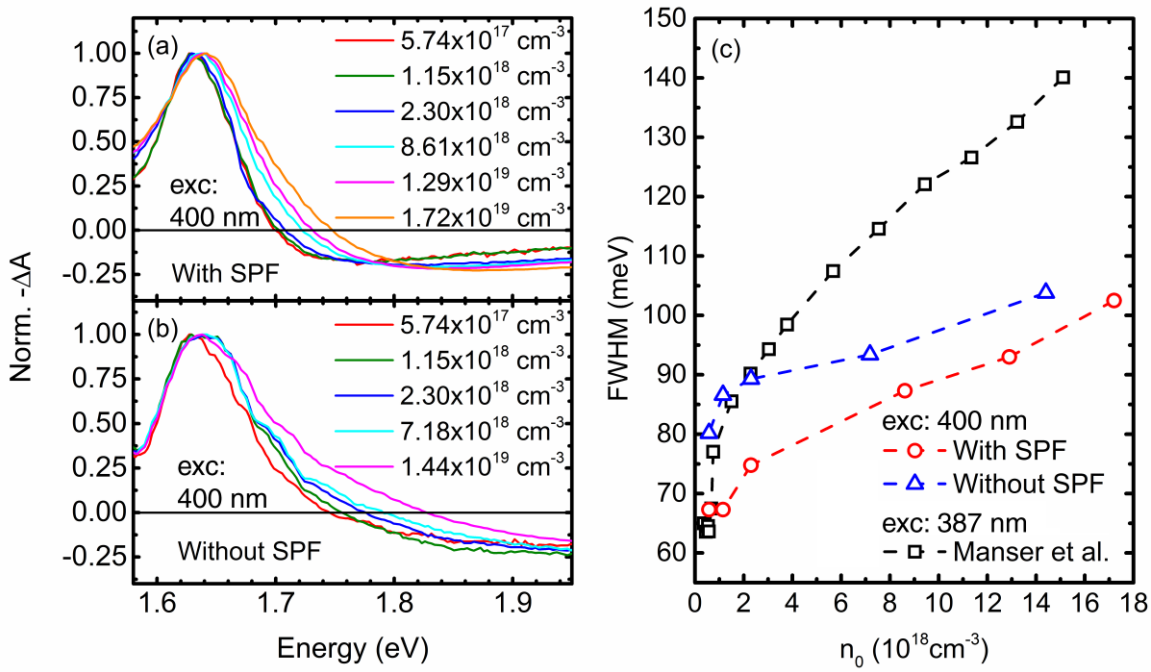

Figure 5| Normalized TA spectra at PB2 at (5±1 ps) following 400 nm photoexcitation at different pump fluence with the spectra taken with **(a)** and without **(b)** the 750 nm SPF, respectively. The corresponding carrier densities, n_0 are given in the legend. **(c)** A plot of PB2's FWHM extracted from **(a)** and **(b)** as a function of n_0. Black open squares are data obtained from a recent publication[22] under 387 nm photoexcitation.

Figure 5 shows the pump-power dependent TA spectra of the sample at (5±1 ps) after photoexcitation with 400 nm with (Fig. 5 (a)) and without (Fig. 5 (b)) the 750 nm SPF in the HELIOS probe path. The absence of the SPF has a profound influence on the spectral broadening of the bandedge bleach PB2. From its full-width half maximum (FWHM), carrier-dependent blue shift and broadening of PB2 is considerably much less with the SPF in place - Fig. 5(c). Without the SPF, the probe becomes "pump-like" and the sample is inadvertently subjected to an immense amount of excitation from the residual 800 nm present in the probe (*i.e.*, ~400 μJ/cm^2 for ~250 μm diameter spot). Our HELIOS TAS data (with SPF) contrasts with a recent report on band-filling and dynamic Burstein-Moss shift where the authors had observed very large blue shifts and spectral broadening - Fig. 5(c).[22] Apart from sample differences and photoexcitation at 387 nm vs 400 nm, one crucial distinction is the regenerative amplifier used in that work has a 775 nm fundamental. Should there be any leakage of the residual 775 nm in the WLC probe to the sample, the spectral blue shift and

broadening of PB2 would be greatly exacerbated with the more resonant 775 nm excitation of $CH_3NH_3PbI_3$ tail states.

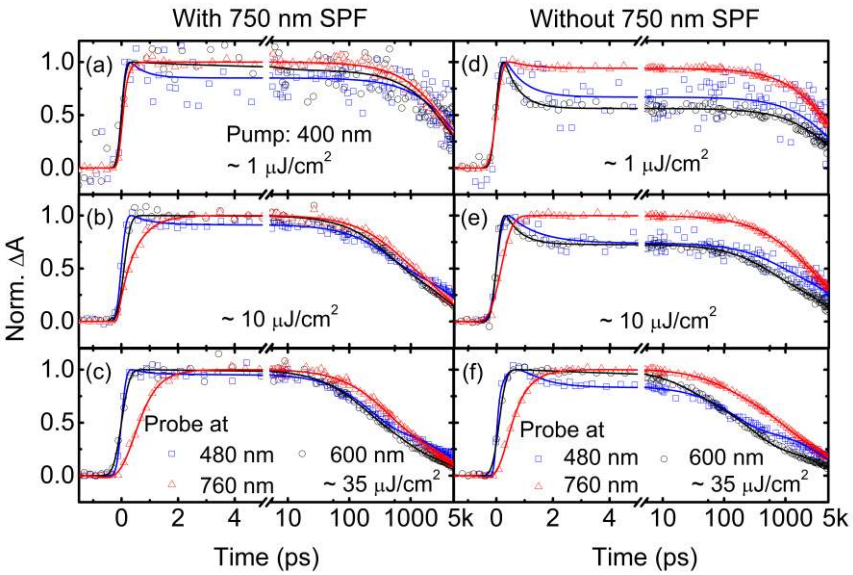

Figure 6 | 400 nm pumped TA kinetics probed at 480 nm (blue), 600 nm (black) and 760 nm (red) under different pump fluence. Left (Right) panels show the results obtained with (without) a 750 nm SPF placed before the sample in the WLC probe path.

Figure 6 shows the normalized TA kinetics at PB1 (480 nm), PB2 (760 nm) and PIA (600 nm) following 400 nm photoexcitation with and without the 750 nm SPF in our HELIOS setup. The absence of the SPF also "wreaks havoc" on the decay transients with large discrepancies in the recovery kinetics/relaxation dynamics at the two probe wavelengths of 480 nm (blue) and 760 nm (red) – Fig 6 (d)-(f). With the SPF in place, the recovery kinetics over the 10 ps to few ns timescale are rather similar – Fig 6 (a)-(c). Focusing on 10 μJ/cm^2 excitation (Fig. 6(b)), at early times of 1-2 ps, the hot carrier cooling process is evident with the SPF in place. This is the concomitant rise of the 760 nm (red) trace and the decay of the 480 nm (blue) trace as the carriers cool from 480 nm to the bandedge proposed in the dual valence band model.[8] However, without the SPF, these signatures will be obscured (Fig. 6(e)) showing equally fast rise times. Our HELIOS TAS results (with SPF) differ greatly from another recent report[34] where the authors had noted: (i) the absence of carrier cooling from 480 nm level to the band edge; and (ii) the presence of a large discrepancy in the recovery kinetics at 480 nm and 760 nm. One possibly for the different observations could be due to the absence of the SPF.

Similarly, without the SPF, large discrepancies in PB1, PB2 and PIA signatures are also evident in the recovery kinetics following 600 nm photoexcitation - Fig. 7 (d)-(f). Likewise, with the SPF in place, the recovery kinetics over the 10 ps to few ns timescale are rather similar – Fig 7 (a)-(c). Here, for the 600 nm pump, we took notice of a detail previously not observed in our earlier work[8] – a small concomitant rise of the 760 nm (red) trace and the decay of the 480 nm (blue) trace at early times of 1-2 ps (Fig. 7(b)). This simultaneous rise

and fall signature becomes more prominent with increased pump excitation at 35 μJ/cm^2 (Fig. 7(c)). We attribute this difference to the differences in our sample preparation in our earlier work[8] (*i.e.*, shorter annealing time and vacuum evaporation discussed earlier – Section 3.1). This simultaneous rise/fall signature at 600 nm pump was also observed by Moser's group (published in Arianna Marchioro's PhD dissertation – reproduced in Fig. 8(c)) where a dual conduction band and dual valence band model was proposed.[32]

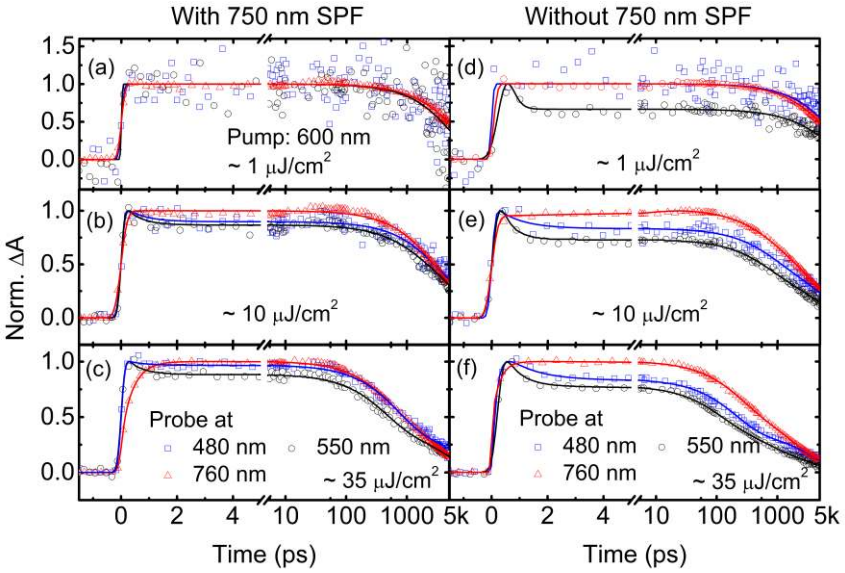

Figure 7 | 600 nm pumped TA kinetics probed at 480 nm (blue), 550 nm (black) and 760 nm (red) under different pump fluence. Left (Right) panel shows the results obtained with (without) a 750 nm SPF placed before the sample in the WLC probe path.

Lastly, apart from the SPF issue and the influence from sample preparation, the detector type could also potentially affect one's TAS data. The SNR of array detectors is typically poorer than point detectors (by as much as 1 order under similar data collection conditions). Small changes like the concomitant rise/decay discussed earlier could also be easily obscured if insufficient time is allocated for data acquisition and signal averaging – Fig. 8. In a bid to improve the SNR, users may therefore be tempted to increase the excitation fluence. This will in turn affect the relaxation dynamics with more contributions from the bimolecular recombination lifetimes (see earlier discussion on the relaxation dynamics). The best approach would be to keep the excitation fluence low to minimize the multiparticle processes while allocating more time for data acquisition and signal averaging.

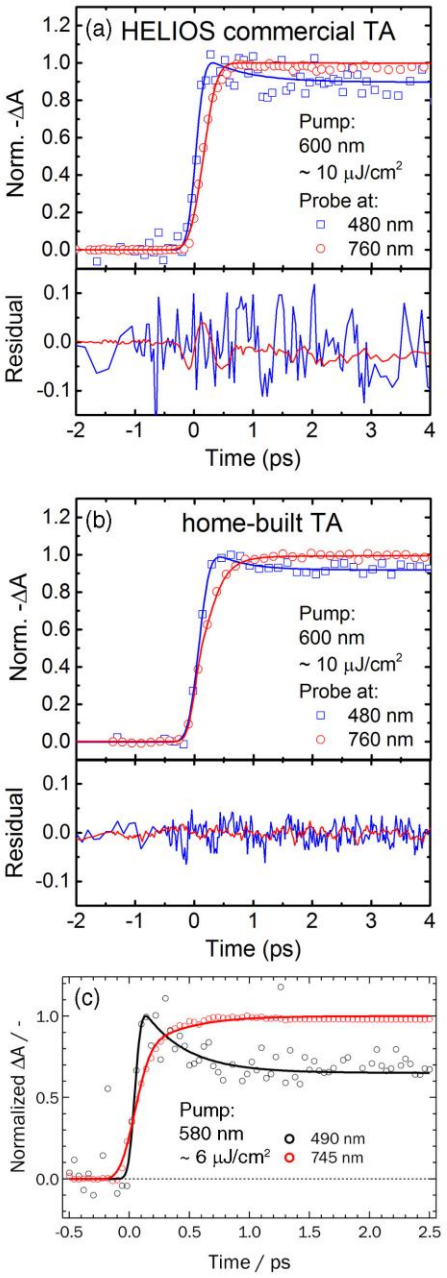

Figure 8 | Comparison of the decay transients for 480 nm (blue) and 760 nm (red) trace at early times collected using (a) HELIOS TAS (with array detector) and (b) home-built TAS (with point detector) with pump excitation at 600 nm at 10 μJ/cm^2. The SNR in the latter is better – evident from the smaller residuals from the fit. Both data sets were collected in a comparable amount of time. (c) TA data from ref[32] – Reproduced with permission from ref. [[32]]. Copyright 2014 [EPFL].

4. Conclusions and Outlook

In summary, we have provided a concise account of the photophysical processes in $CH_3NH_3PbI_3$. Presently, the origin of PB1 is still divergent with various groups possibly measuring different aspects of the same theme. There is also a lack of a detailed model that could account for all these spectral signatures. We have highlighted some potential issues of

TAS and identified some experimentation, sample preparation and treatment factors that could influence the dynamics and the interpretation. In particular, the absence of the 750 nm SPF in the probe will adversely affect the spectral features and kinetics. This could possibly account for some of the differing views and interpretations. Although TAS can provide considerable insights into the ground and excited state dynamics in $CH_3NH_3PbI_3$ films, there are limitations to extrapolating their findings to the actual performance of perovskite solar cells. It is important to note that their device architectures are more complex than in neat films where the morphology, series and shunt resistances, interfacial traps and band alignments *etc.* can have significant influence on the power conversion efficiency (PCE). A complex interplay of these factors is at work in a real device and need not be reflected in the TA findings of neat films. One should avoid over-generalizing and drawing conclusions based on UOS studies alone. UOS studies should be complemented with energetics investigation, materials and device characterization to gain a complete picture. As the field progresses to more complicated mixed perovskites (*e.g.*, $CH_3NH_3Sn_{1-x}Pb_xI_3$, mixed $CH_3NH_3PbBr_3$/$HC(NH_2)_2)PbI_3$) and lead-free systems (*e.g.*, $CH_3NH_3SnI_3$), there is greater urgency to thoroughly characterize and establish $CH_3NH_3PbI_3$ as the model system. To this end, possibly round-robin studies of properly sealed standard $CH_3NH_3PbI_3$ films prepared by leading materials laboratories could be circulated among the various photophysics/photochemistry groups for benchmarking. In the foreseeable future, UOS techniques, especially TAS will continue to play a leading role in uncovering the photophysical mechanisms and charge dynamics in novel halide perovskite systems. Commercial instrumentation will make the TAS technique accessible to even more groups and open up more avenues of research that will provide new insights into the underlying photophysics.

Acknowledgements

Financial support from Nanyang Technological University start-up grants M4080514 and M4081293; the Ministry of Education AcRF Tier 1 grant RG101/15, and Tier 2 grants MOE2013-T2-1-081 and MOE2014-T2-1-044; and from the Singapore National Research Foundation through the Singapore–Berkeley Research Initiative for Sustainable Energy (SinBeRISE) CREATE Program and the Competitive Research Program NRF2014NRF-CRP002-036 is gratefully acknowledged.

Biographical Information Dr. **Tze Chien Sum** is an Associate Professor at the Division of Physics and Applied Physics (PAP), School of Physical and Mathematical Sciences (SPMS), Nanyang Technological University (NTU); where he leads the Femtosecond Dynamics Laboratory. He received his Ph.D. in Physics from the National University of Singapore (NUS) in 2005. His present research focuses on investigating light matter interactions; energy

and charge transfer mechanisms; and probing carrier and quasi-particle dynamics in a broad range of emergent nanoscale and light harvesting systems.

Dr **Nripan Mathews** is an Assistant Professor at the School of Materials Engineering in NTU. He pursued his PhD at a joint Commissariat à l'énergie atomique (CEA) – Centre national de la recherche scientifique (CNRS) – Universite de Pierre et Marie Curie (Paris VI University) laboratory in 2008. His research focuses on a wide variety of novel materials (metal oxides, organic semiconductors, graphene, carbon nanotubes, sulfides, and selenides) and novel morphologies (one dimensional structures such as nanowires and nanotubes, thin films as well as two dimensional nanosheets) produced through a range of fabrication procedures.

Dr. **Guichuan Xing** is a Senior Postdoctoral Research Fellow at the Femtosecond Dynamics Laboratory at PAP, SPMS, NTU, Singapore. He received his Ph.D. in physics from NUS in 2011. His research interests are in the development and application of ultrafast nonlinear optical probes and analysis methods to study novel organic and inorganic materials based optoelectronic devices.

Mr **Swee Sien Lim** received his B.S. degree in Applied Physics from NTU in 2013 and continued as a Ph.D. candidate under the supervision of A/P Tze Chien Sum. His research focuses on probing the ultrafast charge carrier dynamics in perovskite solar cells and understanding the intrinsic photophysical properties of perovskites.

Mr **Wee Kiang Chong** received his B.S. degree in Applied Physics from NTU in 2013 and is a PhD candidate at NTU under the supervision of A/P Tze Chien Sum. His current research includes understanding the carrier recombination and photon amplification mechanisms in light emitting perovskites.

Mr **David Giovanni** is currently a PhD candidate at NTU, under the supervision of Ast/P Nripan Mathews and A/P Tze Chien Sum. He received his B.Sc. degree in Physics from NTU in 2014. His current research focuses on exploration and fundamental study of novel ultrafast spin phenomena and dynamics in organic-inorganic hybrid perovskite for applications in opto-spintronics.

Dr **Herlina Arianita Dewi** received her Ph.D. from NTU in 2014. Currently she is working as a research fellow in Energy Research Institute @ NTU (ERI@N) Singapore. Her main research interest is focused on organometallic halide perovskites for photovoltaic applications.

References

(1) Hong, X.; Ishihara, T.; Nurmikko, A. V. Photoconductivity and Electroluminescence in Lead Iodide Based Natural Quantum-Well Structures. *Solid State Commun* **1992**, *84*, 657-661.

(2) Kagan, C. R.; Mitzi, D. B.; Dimitrakopoulos, C. D. Organic-inorganic hybrid materials as semiconducting channels in thin-film field-effect transistors. *Science* **1999**, *286*, 945-947.

(3) Kojima, A.; Teshima, K.; Shirai, Y.; Miyasaka, T. Organometal halide perovskites as visible-light sensitizers for photovoltaic cells. *J Am Chem Soc* **2009**, *131*, 6050-6051.

(4) Kim, H. S.; Lee, C. R.; Im, J. H.; Lee, K. B.; Moehl, T.; Marchioro, A.; Moon, S. J.; Humphry-Baker, R.; Yum, J. H.; Moser, J. E.; Gratzel, M.; Park, N. G. Lead Iodide Perovskite Sensitized All-Solid-State Submicron Thin Film Mesoscopic Solar Cell with Efficiency Exceeding 9%. *Sci Rep-Uk* **2012**, *2*, 591.

(5) Lee, M. M.; Teuscher, J.; Miyasaka, T.; Murakami, T. N.; Snaith, H. J. Efficient Hybrid Solar Cells Based on Meso-Superstructured Organometal Halide Perovskites. *Science* **2012**, *338*, 643-647.

(6) Burschka, J.; Pellet, N.; Moon, S. J.; Humphry-Baker, R.; Gao, P.; Nazeeruddin, M. K.; Gratzel, M. Sequential deposition as a route to high-performance perovskite-sensitized solar cells. *Nature* **2013**, *499*, 316-319.

(7) Liu, M. Z.; Johnston, M. B.; Snaith, H. J. Efficient planar heterojunction perovskite solar cells by vapour deposition. *Nature* **2013**, *501*, 395-398.

(8) Xing, G. C.; Mathews, N.; Sun, S. Y.; Lim, S. S.; Lam, Y. M.; Gratzel, M.; Mhaisalkar, S.; Sum, T. C. Long-Range Balanced Electron- and Hole-Transport Lengths in Organic-Inorganic CH3NH3PbI3. *Science* **2013**, *342*, 344-347.

(9) Stranks, S. D.; Eperon, G. E.; Grancini, G.; Menelaou, C.; Alcocer, M. J. P.; Leijtens, T.; Herz, L. M.; Petrozza, A.; Snaith, H. J. Electron-Hole Diffusion Lengths Exceeding 1 Micrometer in an Organometal Trihalide Perovskite Absorber. *Science* **2013**, *342*, 341-344.

(10) Wehrenfennig, C.; Eperon, G. E.; Johnston, M. B.; Snaith, H. J.; Herz, L. M. High Charge Carrier Mobilities and Lifetimes in Organolead Trihalide Perovskites. *Adv Mater* **2014**, *26*, 1584-1589.

(11) Ponseca, C. S.; Savenije, T. J.; Abdellah, M.; Zheng, K. B.; Yartsev, A.; Pascher, T.; Harlang, T.; Chabera, P.; Pullerits, T.; Stepanov, A.; Wolf, J. P.; Sundstrom, V. Organometal Halide Perovskite Solar Cell Materials Rationalized: Ultrafast Charge Generation, High and Microsecond-Long Balanced Mobilities, and Slow Recombination. *J Am Chem Soc* **2014**, *136*, 5189-5192.

(12) Xing, G.; Mathews, N.; Lim, S. S.; Yantara, N.; Liu, X.; Sabba, D.; Grätzel, M.; Mhaisalkar, S.; Sum, T. C. Low-temperature solution-processed wavelength-tunable perovskites for lasing. *Nat Mater* **2014**, *13*, 476-480.

(13) Even, J.; Pedesseau, L.; Jancu, J. M.; Katan, C. Importance of Spin-Orbit Coupling in Hybrid Organic/Inorganic Perovskites for Photovoltaic Applications. *J. Phys. Chem. Lett.* **2013**, *4*, 2999-3005.

(14) De Wolf, S.; Holovsky, J.; Moon, S.-J.; Löper, P.; Niesen, B.; Ledinsky, M.; Haug, F.-J.; Yum, J.-H.; Ballif, C. Organometallic Halide Perovskites: Sharp Optical Absorption Edge and Its Relation to Photovoltaic Performance. *J. Phys. Chem. Lett.* **2014**, *5*, 1035-1039.

(15) Sum, T. C.; Chen, S.; Xing, G.; Liu, X.; Wu, B. Energetics and dynamics in organic–inorganic halide perovskite photovoltaics and light emitters. *Nanotechnology* **2015**, *26*, 342001.

(16) D'Innocenzo, V.; Grancini, G.; Alcocer, M. J. P.; Kandada, A. R. S.; Stranks, S. D.; Lee, M. M.; Lanzani, G.; Snaith, H. J.; Petrozza, A. Excitons versus free charges in organo-lead tri-halide perovskites. *Nat Commun* **2014**, *5*, 3586.

(17) Saba, M.; Cadelano, M.; Marongiu, D.; Chen, F. P.; Sarritzu, V.; Sestu, N.; Figus, C.; Aresti, M.; Piras, R.; Lehmann, A. G.; Cannas, C.; Musinu, A.; Quochi, F.; Mura, A.; Bongiovanni, G. Correlated electron-hole plasma in organometal perovskites. *Nat Commun* **2014**, *5*, 5049.

(18) Miyata, A.; Mitioglu, A.; Plochocka, P.; Portugall, O.; Wang, J. T.-W.; Stranks, S. D.; Snaith, H. J.; Nicholas, R. J. Direct measurement of the exciton binding energy and effective masses for charge carriers in organic-inorganic tri-halide perovskites. *Nat Phys* **2015**, *11*, 582-587.

(19) Sheng, C. X.; Zhang, C.; Zhai, Y. X.; Mielczarek, K.; Wang, W. W.; Ma, W. L.; Zakhidov, A.; Vardeny, Z. V. Exciton versus Free Carrier Photogeneration in Organometal Trihalide Perovskites Probed by Broadband Ultrafast Polarization Memory Dynamics. *Phys Rev Lett* **2015**, *114*, 116601.

(20) Savenije, T. J.; Ponseca, C. S.; Kunneman, L.; Abdellah, M.; Zheng, K. B.; Tian, Y. X.; Zhu, Q. S.; Canton, S. E.; Scheblykin, I. G.; Pullerits, T.; Yartsev, A.; Sundstrom, V. Thermally Activated Exciton Dissociation and Recombination Control the Carrier Dynamics in Organometal Halide Perovskite. *J. Phys. Chem. Lett.* **2014**, *5*, 2189-2194.

(21) Klimov, V. I.; Mikhailovsky, A. A.; McBranch, D. W.; Leatherdale, C. A.; Bawendi, M. G. Quantization of Multiparticle Auger Rates in Semiconductor Quantum Dots. *Science* **2000**, *287*, 1011-1013.

(22) Manser, J. S.; Kamat, P. V. Band filling with free charge carriers in organometal halide perovskites. *Nat Photonics* **2014**, *8*, 737-743.

(23) Price, M. B.; Butkus, J.; Jellicoe, T. C.; Sadhanala, A.; Briane, A.; Halpert, J. E.; Broch, K.; Hodgkiss, J. M.; Friend, R. H.; Deschler, F. Hot-carrier cooling and photoinduced refractive index changes in organic-inorganic lead halide perovskites. *Nat Commun* **2015**, *6*, 8420.

(24) Yang, Y.; Ostrowski, D. P.; France, R. M.; Zhu, K.; van de Lagemaat, J.; Luther, J. M.; Beard, M. C. Observation of a hot-phonon bottleneck in lead-iodide perovskites. *Nat Photonics* **2015**, *advance online publication*.

(25) Grancini, G.; Srimath Kandada, A. R.; Frost, J. M.; Barker, A. J.; De Bastiani, M.; Gandini, M.; Marras, S.; Lanzani, G.; Walsh, A.; Petrozza, A. Role of microstructure in the electron–hole interaction of hybrid lead halide perovskites. *Nat Photonics* **2015**, *9*, 695-701.

(26) deQuilettes, D. W.; Vorpahl, S. M.; Stranks, S. D.; Nagaoka, H.; Eperon, G. E.; Ziffer, M. E.; Snaith, H. J.; Ginger, D. S. Impact of microstructure on local carrier lifetime in perovskite solar cells. *Science* **2015**, *348*, 683-686.

(27) Sum, T. C.; Mathews, N. Advancements in perovskite solar cells: photophysics behind the photovoltaics. *Energy Environ Sci* **2014**, *7*, 2518-2534.

(28) Johnston, M. B.; Herz, L. M. Hybrid Perovskites for Photovoltaics: Charge-Carrier Recombination, Diffusion, and Radiative Efficiencies. *Acc Chem Res* **2015**.

(29) Saba, M.; Quochi, F.; Mura, A.; Bongiovanni, G. Excited State Properties of Hybrid Perovskites. *Acc Chem Res* **2015**.

(30) Lanzani, G.: *The Photophysics behind Photovoltaics and Photonics*; Wiley-VCH: Singapore, 2012.

(31) Ruckebusch, C.; Sliwa, M.; Pernot, P.; de Juan, A.; Tauler, R. Comprehensive data analysis of femtosecond transient absorption spectra: A review. *J Photochem Photobiol C* **2012**, *13*, 1-27.

(32) Marchioro, A. Interfacial Charge Transfer Dynamics in Solid-State Hybrid Organic-Inorganic Solar Cells. Ph.D. Thesis, École polytechnique fédérale de Lausanne, 2014.

(33) Wang, L.; McCleese, C.; Kovalsky, A.; Zhao, Y.; Burda, C. Femtosecond Time-Resolved Transient Absorption Spectroscopy of CH3NH3PbI3 Perovskite Films: Evidence for Passivation Effect of PbI2. *J Am Chem Soc* **2014**, *136*, 12205-12208.

(34) Stamplecoskie, K. G.; Manser, J. S.; Kamat, P. V. Dual nature of the excited state in organic-inorganic lead halide perovskites. *Energy Environ Sci* **2015**, *8*, 208-215.

(35) Tanaka, K.; Takahashi, T.; Ban, T.; Kondo, T.; Uchida, K.; Miura, N. Comparative study on the excitons in lead-halide-based perovskite-type crystals CH3NH3PbBr3CH3NH3PbI3. *Solid State Commun* **2003**, *127*, 619-623.

(36) Even, J.; Pedesseau, L.; Katan, C. Analysis of Multivalley and Multibandgap Absorption and Enhancement of Free Carriers Related to Exciton Screening in Hybrid Perovskites. *J Phys Chem C* **2014**, *118*, 11566-11572.

(37) Leguy, A. M. A.; Azarhoosh, P.; Alonso, M. I.; Campoy-Quiles, M.; Weber, O. J.; Yao, J.; Bryant, D.; Weller, M. T.; Nelson, J.; Walsh, A.; van Schilfgaarde, M.; Barnes, P. R. F. Experimental and theoretical optical properties of methylammonium lead halide perovskites. *Nanoscale* **2016**.

(38) Jeon, N. J.; Noh, J. H.; Kim, Y. C.; Yang, W. S.; Ryu, S.; Il Seol, S. Solvent engineering for high-performance inorganic-organic hybrid perovskite solar cells. *Nat Mater* **2014**, *13*, 897-903.